Resonance Raman Studies of Heme Axial Ligation in H93G Myoglobin

Stefan Franzen,*,† Steven G. Boxer,‡ R. Brian Dyer,§ and William H. Woodruff||

Department of Chemistry, North Carolina State University, Raleigh, North Carolina 27695-8420, Department of Chemistry, Stanford University, Stanford, California 94305, and Bioscience and Biotechnology Group, Los Alamos National Laboratory, Los Alamos, New Mexico 87545

Received: March 31, 2000; In Final Form: August 25, 2000

The resonant Raman active mode identified in numerous studies as the heme iron−histidine stretch has been systematically investigated in the Raman spectrum of 15 exogenous ligands to the heme iron in the myoglobin proximal cavity mutant H93G. Mutation of the native histidine 93 of myoglobin to glycine (H93G) creates a cavity at the heme iron that can be filled with exogenous ligands. Substituted imidazoles and pyridines were introduced into the cavity at the heme iron of the deoxy ferrous H93G myoglobin by dialysis. Raman bands attributed to in-plane modes of the heme are unaffected by the change in heme−iron ligation. However, the Raman active band in the 180−250 cm^{-1} region ascribed to an iron−ligand out-of-plane mode is highly dependent on the identity of the axial ligand. Information on the normal mode was obtained using isotopically labeled imidazole, pyridine, and 1-methyl and 2-methyl imidazole. Relatively small isotope effects are observed for the heme−iron ligands imidazole H93G(Im) and pyridine H93G(Pyr). We have examined models for the normal mode based on three-body, six-body, and 38-body calculations of the FG matrix. These models indicate that the potential energy distribution of the axial-ligand out-of-plane normal mode observed in the region from 180 to 245 cm^{-1} has a significant contribution from iron−ligand (Fe−L) stretching (50−70%) but also from significant iron−heme doming. Using the normal coordinate analysis to correct for differences in ligand mass, we have compared the frequencies of the ligands as a function of their basicity. Although the iron−ligand force constant is linearly proportional to ligand basicity at $pK_a > 5$, the correlation is less pronounced at lower pK_a.

Heme axial ligation by histidine is a key determinant of the reactivity of the iron in globins, peroxidases, and oxidases. A Raman active band observed in the 180−250 cm^{-1} range in the deoxy ferrous form of various histidine-ligated heme proteins has provided key evidence for mechanisms of control over the activation of bound oxygen.[6−9] Experimental resonant Raman studies of isotopically labeled hemes, iron, and ^{15}N-labeled myoglobin proteins with Soret band excitation ($\lambda_{ex} \approx 430$−435 nm) have shown that the stretching of the iron−histidine bond is a major contributor to the potential energy distribution of the iron−histidine normal mode.[1−3] The designation of this band as the iron−histidine normal mode has led to systematic studies of the differences in heme proteins and the reactivity of the heme iron in terms of the frequency of the iron−histidine vibration. The reversible oxygen binding of globins is facilitated by a neutral histidine trans to the oxygen binding site on the heme iron. The frequency of the iron−histidine mode has been empirically correlated with both the diatomic ligand binding affinity in hemoglobin[10,11] and the reactivity of the peroxidases.[8] In hemoglobin, a low frequency ($\nu \approx 216$ cm^{-1}) for the band is associated with the low-affinity T state while the high-affinity R state has a higher frequency, similar to that of noncooperative myoglobin ($\nu \approx 222$ cm^{-1}).[6,11] The frequency of the iron−histidine band is increased from the 220 cm^{-1} range in globins to 245 cm^{-1} in peroxidases, consistent with a stronger interaction between the histidine ligand and the heme iron, due perhaps to a more negatively charged imidazole.[12,13] The iron−histidine bond in guanylate cyclase is thought to be strained or weak in this enzyme since the binding of NO ruptures the iron−histidine bond at its iron−histidine band frequency of 206 cm^{-1}, which is significantly lower than in myoglobin.[14] The low frequency of the iron−histidine band ($\nu \approx 193$−214 cm^{-1}) in oxidases[2,15,16] is consistent with weak hydrogen bonding.[17,18]

In this paper, we present a resonant Raman study of the iron−ligand out-of-plane mode in the proximal cavity mutant of myoglobin H93G. The single-point mutation of the native histidine 93 to glycine (H93G) creates a cavity at the heme iron that can be filled with a number of exogenous ligands.[4,5] In this study, we have used a range of substituted imidazoles and pyridines, shown in Table 1. There are now cavity mutants of several heme enzymes[4,5,19−21] demonstrating the general utility of studying the heme active site using non-native heme−iron ligands in heme proteins. The H93G mutant of myoglobin has the advantage that the proximal cavity is relatively nonpolar, allowing a systematic study of a range of exogenous ligands. In addition, a comparison of several isotopomers of different ligands allows information on the normal mode description to be obtained. We present an analysis based on force field data that elucidate the relative contributions of iron out-of-plane motion, porphyrin ring deformations, and internal degrees of freedom of the ligand to the potential energy distribution of the normal mode observed in the Raman spectrum. A three-body model treats the heme, iron, and ligand as rigid masses. A six-body model includes the off-axis tilting of the iron−ligand bond. A 38-body model explicitly treats the entire porphyrin ring with β substituents (but ignores hydrogens and the internal degrees of freedom of the heme peripheral substituents). The

† North Carolina State University.
‡ Stanford University.
§ Los Alamos National Laboratory.

10.1021/jp001231v CCC: $19.00
Published on Web 10/12/2000

TABLE 1: Observed Frequencies of 17 Ligands to Deoxyferrous Heme Iron in the Proximal Cavity of H93G Myoglobin[a]

ligand	Fe−L (cm^{-1})	pK_a	MW	Soret
imidazole	225	6.65	68	431
1-Me Im	219, 231	7.33	82	428
2-Me Im	217	7.56	82	430.5
4-Me Im	221	7.22	82	433
1,2-diMe Im	225	7.85	96	429
2,4-diMe Im	197	−	96	432.5
2-ethyl Im	219.5	7.70	97	431
4-CH_2OH Im	227.5	−	98	430
4-Br Im	196	−	147	426
4-Br,2-Me Im	180	−	159	431
pyridine	207	5.22	79	424
3-F Pyr	201	2.97	97	−
3-Me Pyr	207	5.6	93	−
3-Br Pyr	201	2.84	158	−
4-Me Pyr	194	5.98	93	−

[a] Represents the mass effect of various ligands referenced to the mass and frequency of H93G(Im).

analysis allows us to extract the iron−ligand stretching force constant of a variety of exogenous ligands for comparison.

Experimental Section

The H93G protein was obtained by standard methods. Samples of H93G myoglobin with different ligands were prepared by dialysis, as discussed previously.[5] The samples were prepared in 50 mM phosphate buffer solution at pH 7.0. The deoxy form of myoglobin was prepared by dilution into deoxygenated buffer, followed by reduction with excess dithionite. Solutions were placed in a spinning NMR tube at ambient temperature. Isotopic shifts were measured by repetitively placing the natural abundance and isotopically lableled samples in the laser beam for alternating 2 min data acquisition periods. A typical data set consisted of 10 repetitions for a total of 20 min of data acquisition time. The magnitude of the isotope shifts is based on fits to the line shape with two Gaussian functions (see Supporting Information). It is well-known that there are several in-plane Raman bands in the region of the iron−ligand out-of-plane band.[22,23] These can be fit by a number of Gaussians or Lorentzians to separate the isotopically shifted peak from other heme vibrational modes in the spectral region.[23]

Resonance Raman experiments were conducted using a Coherent 590 dye laser (Stilbene-420 dye) pumped by the UV lines of a Coherent Innova 400 argon ion laser. The laser frequency was tuned to between 430 and 435 nm. As shown in Table 1, the laser frequency corresponds to the λ_{max} of the Soret band for the deoxy H93G(L) species where L represents the various ligands. Typical laser powers were 10−20 mW. Scattered light was collected by an *f*/1 5 cm focal length lens and focused on the slit of a SPEX 0.6 monochromator operating as a spectrograph to disperse the light with 2.5 cm^{-1} resolution onto a Photometrics CCD camera.

The models we have studied include a 3-body linear model, a simple 6-body model with C_{4v} symmetry, and a 38-body model of the porphyrin ring with β substituents, as shown in Figure 1. The three-body model shown in Figure 1A is a gross simplification that allows general trends in the iron-ring stretching force constant relative to the iron−ligand force constant. The six-body model shown in Figure 1B contains the essential features of iron geometry in five-coordinate deoxy Fe(II) complexes and therefore allows us to visualize the basic mode types that involve the motion of the iron and the axial ligand with relation to the heme plane. The inclusions of the porphyrin in a porphine model

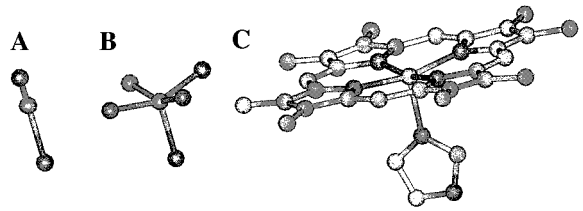

Figure 1. Three models used to analyze iron−ligand out-of-plane normal modes in heme: (A) the three-body model consists of three different masses connected by two springs with different force constants; (B) the six-body C_{4v} symmetry model consists of three difference masses and four masses that represent the porphyrin macrocycle identical in their stretching and bending force constants; (C) the 38-body model can have symmetry as high C_{2v} and consists of a porphyrin ring with β substitutents. Hydrogens are not included in the model.

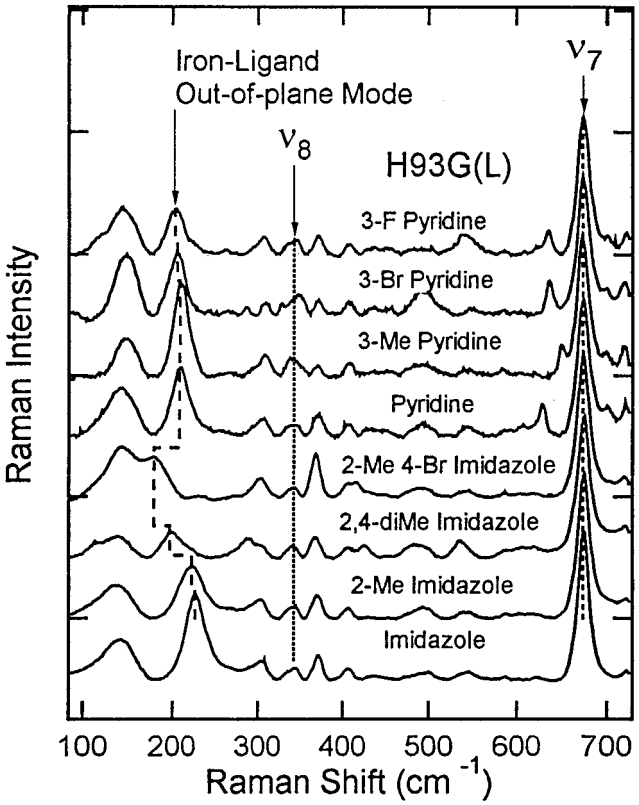

Figure 2. Resonance Raman spectra for deoxyferrous H93G myoglobin shown with various ligands L in the proximal cavity. The iron−ligand out-of-plane mode depends strongly on the ligand. The mode at ∼140 cm^{-1} has not been assigned, and although substantially different than the wild type, this mode does not appear to shift substantially for different ligand adducts. The totally symmetric heme in-plane mode ν_7 does not depend on the identity of the proximal ligand.

(without hydrogens) and of all ligand coordinates produced a more realistic normal mode model, shown in Figure 1C. Frequencies for all these models can be determined by diagonalizing the FG matrix.[24] In the 38-body model, there are a large number of in-plane normal modes. We have relied on the normal-mode analysis of Li et al., used to derive the in-plane force field parameters based on experimental studies of isotopically labeled nickel octaethyl porphyrin, NiOEP.[25]

Results

The resonance Raman spectra of the low-frequency region of deoxy ferrous H93G with various ligands are shown in Figure 2. There are several modes in the low-frequency region that show some dependence on the identity of the axial ligand. The

largest effect is observed for the iron−ligand out-of-plane band frequencies from 180 to 240 cm^{-1}. These frequencies are given in Table 1 along with the pK_a's of the ligands. The data in Table 1 show that the iron−ligand out-of-plane band frequency tends to increase with ligand basicity, in contrast to the results of earlier studies on heme model systems. [26] However, this is a rough correlation, and a normal-mode analysis of the vibration between 180 and 240 cm^{-1} is required to quantitatively correct for the difference in mass and determine whether there is a correlation of the iron−ligand force constant with pK_a.

There are also changes in two other bands in the low-frequency region below 340 cm^{-1}. All the ligand substitutions into the proximal cavity of H93G appear to affect the band near ∼140 cm^{-1} to some extent. This Raman band has not been assigned, although it is known that its depolarization ratio ($\rho \approx 0.4$) is significantly larger than that of the ∼218 cm^{-1} iron−histidine out-of-plane band ($\rho \approx 0.15$).[27] In agreement with previous reports on wild-type myoglobin, the depolarization ratio of the 140 cm^{-1} band has been found to be significantly larger than that of the 225 cm^{-1} iron−ligand mode in H93G(Im) ($\rho < 0.18$, data not shown). The isotopic shift in the 140 cm^{-1} band is extremely small and was not analyzed. Ligands with a large mass relative to imidazole or large steric bulk affect the spectrum in the 300 cm^{-1} region as well. An additional feature and/or a shift in the 300 cm^{-1} band attributed to γ_7[22] appears in the low-frequency spectra for the ligands H93G(3-Br Pyr) and H93G(2,4-diMe Im).

The isotope shifts of three H93G deoxy adducts in the spectral region from 185 to 265 cm^{-1} are shown in Figures 3−5. The isotope shifts of one isotopomer of imidazole H93G-(d_3-Im) and H93G(Im) are shown in the low-frequency region of the Raman spectra in Figure 3. Fits to the region from 185 to 265 cm^{-1} with up to four Gaussians gave similar results (data not shown). The shift of the peak of the iron−imidazole band at 225 cm^{-1} is 0.9 ± 0.2 cm^{-1} lower for d_3-imidazole substitution and 0.6 ± 0.2 cm^{-1} lower for 1,3-di-^{15}N-imidazole substitution (Table 2). The substitution of d_5-pyridine for pyridine in H93G(Pyr) results is a shift of 1.6 ± 0.3 cm^{-1} in the 207 cm^{-1} band. This is the only isotope shift in the low-frequency Raman spectrum. For the pyridine ligand, there are two large isotope shifts in pyridine Raman bands at 630 and 980 cm^{-1} (data not shown). These two isotope effects indicate that there is resonance enhancement of these internal ring modes of the pyridine upon the $\pi-\pi^*$ excitation of the Soret band of heme. The low-frequency Raman spectra for 2-methyl imidazole and its d_5 isotopomer in H93G(2-Me Im) are shown in Figure 4. A fit of the line shape to a single Gaussian is much poorer than for H93G(Im). A fit to two Gaussians gives a frequency of 217 cm^{-1} and a smaller band of ∼240 cm^{-1}. The 240 cm^{-1} band is also observed in wild-type sperm whale myoglobin but shows some variability in spectra of different ligands in H93G. The isotope shift of the 217 cm^{-1} band upon deuteration, based on these fits, is 5.3 ± 0.3 cm^{-1}, as reported in Table 2. This result is larger than that observed in an early report of isotope effects for perdeutero 2-Me Im ligated metalloporphyrins.[1] If we consider only the peak position, the shift will be 3.7 cm^{-1}, in substantially better agreement with earlier work.[1] The resonance Raman data for isotopically labeled N-methyl imidazole in the low-frequency region show an unusual isotope shift (see Figure 5). The Raman spectrum of deoxy ferrous H93G(N-Me Im) exhibits two bands at 219 and 231 cm^{-1} in the region of the spectrum where a range of other substituted imidazoles and pyridines show only a single peak. However, the double peaks of the bands at 219 and 231 cm^{-1} in Figure 5 appear to coalesce into a single peak in each of two isotopomers of H93G(N-Me Im) (d_2 and 1,3-di-^{15}N N-Me Im). Thus, the shift in each of the two substituted imidazoles is large relative to that of the unsubstituted H93G(Im) and H93G(Pyr). In all the spectra described in this paper, there are no significant differences in the high-frequency region above 1000 cm^{-1} either for different ligands or for various isotopomers (data not shown).

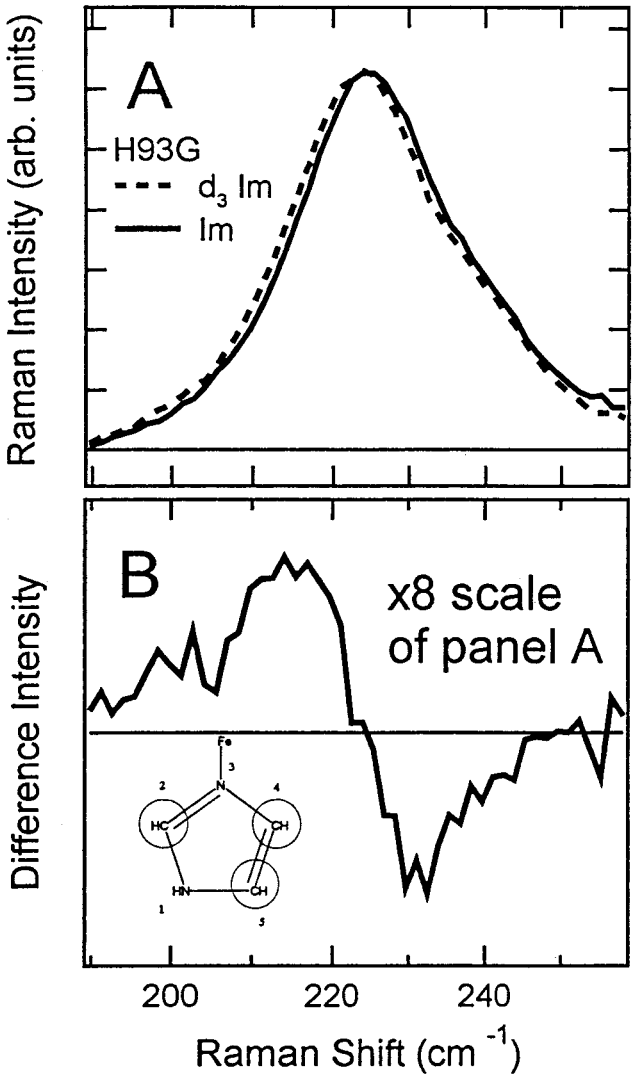

Figure 3. Resonance Raman spectrum of the iron−imidazole out-of-plane mode. The mode at 225 cm^{-1} shifts 0.9 cm^{-1} to a lower frequency upon the isotopic substitution of d_3-imidazole (d_3-Im). A proportionately smaller shift is observed for the 1,3-di-^{15}N imidazole substitution (data not shown). The difference spectrum is shown in panel B.

Analysis

We have investigated the nature of the iron−axial-ligand mode in three geometric models, shown in Figure 1. We compare the results of these model calculations with the two-body harmonic oscillator model indicated by the assignment of the iron−axial-ligand band at ∼219 cm^{-1}, known as ν_{Fe-His}, an iron−histidine stretch. In the two-body model, the masses involved are the iron and the ligand, with a single force constant that corresponds to the iron−ligand bond. The data presented in Figures 4−6 are compared to a two-body harmonic oscillator model for the expected isotope shifts in Table 2. The isotope shifts of H93G(Im) and H93G(Pyr) are significantly smaller than those expected for a two-body harmonic oscillator. However, the isotope shifts of H93G(2-Me Im) and H93G(N-Me Im) are

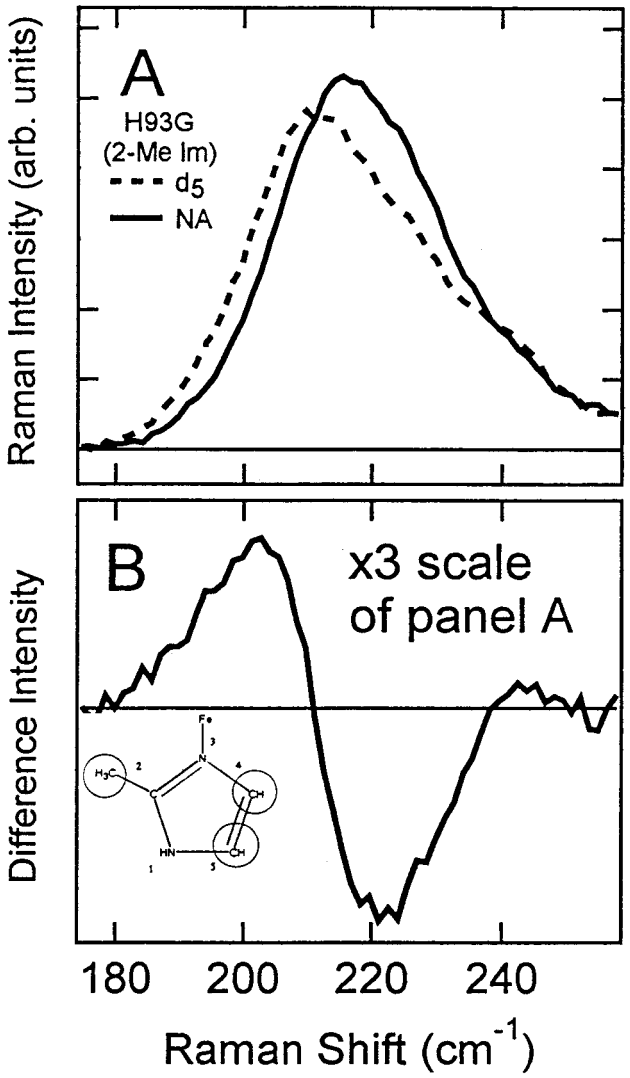

Figure 4. Resonance Raman spectrum of the iron-2-methyl imidazole out-of-plane mode. The mode at 217 cm^{-1} shifts 5.3 cm^{-1} to a lower frequency upon the isotopic substitution of d_5-2-methyl-imidazole (d_5-2-Me-Im). NA stands for natural abundance. The difference spectrum is shown in Figure 5B.

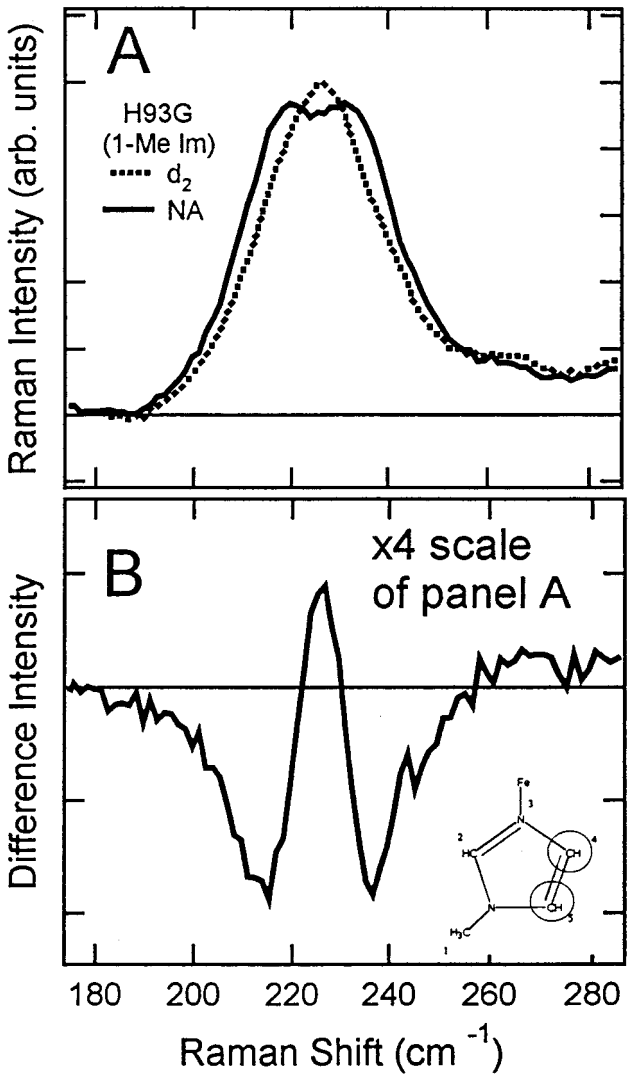

Figure 5. Resonance Raman spectrum of the iron-N-methyl imidazole out-of-plane mode. The mode with two peaks at 219 and 231 cm^{-1} coalesces into a single peak at 225 cm^{-1} upon isotopic substitution of either d_2-N-methyl imidazole (d_2-N-Me-Im). A similar result is observed for 1,3-di-^{15}N-methyl imidazole substitution (data not shown). The difference spectrum is shown in Figure 6B.

larger than expected for the two-body model. This observation is likely to be due to a contribution from the large anharmonicity of these modes. To further analyze these data, we present the frequencies and other relevant aspects of normal mode coordinate analyses of the three-body, six-body, and whole-porphyrin models for the iron−ligand axial vibrational mode.

Discussion

There is widespread agreement with the assignment of the iron−axial-ligand normal mode in the Raman spectra of heme proteins based on the available isotope data.[2,3,28,29] However, the iron ^{54}Fe/^{57}Fe isotope effect, ligand isotope effect, and labeled pyrrole nitrogen ^{15}N/^{14}N isotope effect in myoglobin are all smaller than would be predicted by the two-body harmonic oscillator model, $\Delta\nu = \nu(\sqrt{(\mu/\mu')} - 1)$, where μ is the reduced mass $m_1m_2/(m_1 + m_2)$.[2] In addition, the isotope effect substituting ^{64}Ni in Ni-reconstituted myoglobin also produced an isotope effect smaller than would be expected for a pure two-body Ni−His stretch.[30] Our study provides further direct evidence that a diatomic iron−ligand stretching model is overly simplified. The H93G(Im) data exhibit a 60% discrepancy between the observed (0.9 ± 0.2 cm^{-1} for d_3-Im and 0.6 ± 0.2 cm^{-1} for 1,3-di-^{15}N-Im) and predicted (2.2 and 1.5 cm^{-1}) isotope shifts (see Table 2). The isotope shift observed for d_5-pyridine is 1.6 ± 0.3 cm^{-1}, only ≈60% of the predicted shift of 2.6 cm^{-1} (see Table 2).

TABLE 2: Observed and Calculated (on the basis of a two-body harmonic oscillator model) Isotopic Shifts

H93G(L)	observed	calculated
d_3-Im	0.9	2.2
1,3-di-^{15}N Im	0.6	1.5
d_5-Pyr	1.6	2.6
d_5-2-Me Im	5.3	2.6
d_2-N-Me Im	>9	<1.2
1,3-^{15}N N-Me Im	>9	<1.2

To account for the isotope data using a normal mode coordinate analysis, we need an estimate for the force constants involved. The analysis of in-plane modes of Ni OEP provides a starting point in the Ni−N_p stretching force constant of 1.68 mdyn/Å.[25] Unlike Ni, the high-spin Fe cannot reside in the plane of the heme due to electronic repulsion. Therefore, it is likely that the Fe−N_p force constant is smaller in five-coordinate heme complexes due to the longer Fe−N_p bond in the out-of-plane

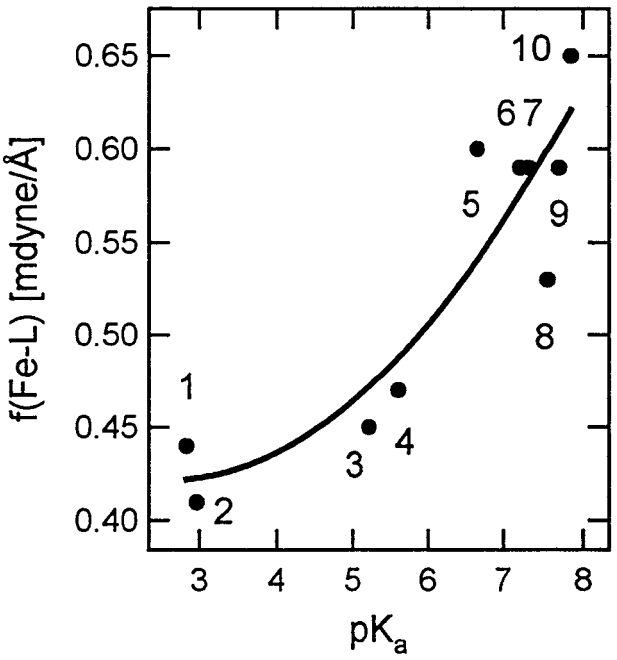

Figure 6. Force constant of ligands obtained from the three-body model for the axial-ligand out-of-plane mode plotted as a function of the ligand pK_a. The curve is a fit to the data using a quadratic function.

geometry. To obtain an initial value, we estimate the axial force constant Fe−L (L is the axial ligand), $f \approx 0.95$ mdyn/Å, using a diatomic harmonic oscillator model ($f \approx \mu\omega^2$) for the Fe−Im mode at 225 cm^{-1}. This value is in reasonable agreement with an estimate based on a bond length/force constant correlation.[31] In heme proteins, estimates for the Fe−N_ϵ distance vary in the range of 2.1−2.3 Å, depending on the crystal structure,[32−34] and high-resolution EXAFS determination yields an estimate of 2.2 Å.[35] On the basis of an empirical correlation derived from a large body of data, we calculate the force constants to be in the range of 1.4−0.5 mdyn/Å, corresponding to distances of 2.1−2.3 Å.[31] The value of 0.95 mdyn/Å for the Fe−L force constant corresponds to a bond length of 2.2 Å. Thus, both the Fe−N_ϵ and the Fe−N_p stretching force constants are <1.5 mdyn/Å. In a three-body model, we require a stretching force constant that represents the axial out-of-plane motion of the iron relative to the heme plane (called Fe−P for Fe−porphyrin). This is a doming motion with respect to the iron coordination geometry, but it is distinct from the doming motion of the porphyrin macrocycle. The Fe−P force constant is the axial projection of the four Fe−N_p force constants. Taking the value of <1.5 mdyn/Å and an angle of ∼30° between the Fe−N_p bond vector and the heme plane, we find the axial component of the four Fe−N_p stretches to be ∼1 mdyn/Å. These considerations indicate a rough parity of the stretching force constant for axial and equatorial (pyrrole nitrogen) ligands. Relative to these stretching force constants, the N_p−Fe−N_p bending force constant of 0.25 mdyn Å^{-1} rad^{-1} found in a recent study of out-of-plane modes of NiOEP is also significant. [25] Similar considerations have been applied to the six-coordinate ferric bis-imidazole OEP complex, $[(ImH)_2Fe(III)OEP]^+$, where significant contributions of doming and asymmetric axial ligand stretching have been observed.[36]

We consider three models: (1) a three-body model treating the porphyrin and ligand as rigid masses, (2) a six-body model including the bending force constants and modeling the porphyrin with four masses in the positions of the pyrrole nitrogens, and (3) a porphyrin model including 10 carbons, 4 nitrogens, and all masses at the C_β positions. In these more realistic models, we will consider various magnitudes for the axial and equatorial Fe−N_p force constants.

TABLE 3: Force Constants, Frequencies, and Potential Energy Distributions for the Three-Body Model with a Single Force Constant of *f*(Fe−L) = *f*(Fe−P)

f (mdyn/Å)	(+) (cm^{-1})	(−) (cm^{-1})	(+) %PED (Fe−L)	(+) %PED (Fe−P)	(−) %PED (Fe−L)	(−) %PED (Fe−P)
4.1	561.0	225.3	100	0	1	99
1.67	358.0	143.8	81	19	4	96
0.66	224.8	88.6	61	39	19	81

Three-Body Model of the Iron−Ligand Out-of-Plane Mode. Given the small magnitude of the force constants for iron ligation, we can begin with the assumption of the separation of the iron ligand stretching coordinate, $f < 1.68$ mdyn/Å, from the high-frequency internal stretches of either the ligand or the heme which have $k \approx 5-10$ mdyn/Å for typical C−C and C−N bonds. The scenario is reduced to three masses connected by two springs, as shown in Figure 1A. The model can be represented as masses labeled L−Fe−P (1−2−3). There are two stretching force constants: $f_{1,2}$ is the iron−ligand (Fe−L) force constant, and $f_{2,3}$ is the iron−porphyrin (Fe−P) force constant. The eigenvalues of a three-body model with $f_{1,2}$ [*f*(Fe−L)], $f_{2,3}$ [*f*(Fe−P)], and three masses are given by

$$\lambda_\pm = \{((m_1+m_2)m_3f_{1,2} + (m_2+m_3)m_1f_{2,3}) \pm [((m_1+m_2)m_3f_{1,2} + (m_2+m_3)m_1f_{2,3})^2 - 4m_1m_2m_3(m_1+m_2+m_3)]^{1/2}\}/2m_1m_2m_3 \quad (1)$$

where the masses are given in atomic mass units and the force constant is given in mdyn/Å. The masses used in the three-body model are heme (488 amu), iron (56 amu), and imidazole (68 amu). To obtain the wavenumber of the vibration, we use $\lambda = 4\pi^2c^2\nu^2$ or ν (in cm^{-1}) $= 1303.9\sqrt{\lambda}$. Since the masses are not equal, the (+) and (−) solutions of the three-body problem are not referred to as symmetric and antisymmetric but, rather, as predominantly Fe−L or Fe−P.

The character of each mode can be described in terms of the potential energy distribution (%PED), the percentage of the potential energy contained in an individual internal coordinate, Fe−L or Fe−P. Table 3 shows a special case of the solution to this three-body model with both force constants equal, $f = f_{1,2}$ [*f*(Fe−L)] = $f_{2,3}$ [*f*(Fe−P)]. For $f = 4.1$ mdyn/Å, there are essentially pure stretching modes that involve only the Fe−L or Fe−P. While this model does produce one mode (−) that agrees with the experimental frequency, the isotope effect is not in agreement. A value of $f = 1.67$ mdyn/Å in the middle row of Table 3 is similar to the value needed to account for the asymmetric axial ligand stretching modes at 319 and 385 cm^{-1} in six-coordinate $[(ImH)_2Fe(III)OEP]^+$ [36] but is not in good agreement with the data for the deoxy heme axial ligand mode considered here. A value of $f = 0.66$ mdyn/Å agrees both with the experimental frequency of 225 cm^{-1} and surprisingly well with the isotope data; the %PED of the Fe−L stretching coordinate is 60%.

The results of a three-body calculation with two different force constants, $f_{1,2} \neq f_{2,3}$, are given in Table 4. The isotope effect of the substitution of the pyrrole nitrogens (i.e., a mass change from 488 to 492 amu) is very small for either of the two modes from this calculation, as shown in Table 4. This effect is due to the large rigid mass of the porphyrin and is in agreement with the experiment. The L isotope effect is small in the predominantly Fe−L mode (+) and is in approximately the correct range. However, the isotope effect of the iron is

TABLE 4: Force Constants, Frequencies, Isotope Effects, and Potential Energy Distributions for the Three-Body Model

force constants		isotopic wavenumber shifts (cm^{-1})				%PED	
f(Fe−L)	f(Fe−P)	n	d_3-Im	^{57}Fe−^{54}Fe	^{15}Np	Fe−L	Fe−P
0.66	0.66	224.8	−1.0	4.7	<0.1	61	39
0.60	0.78	225.5	−0.8	4.9	<0.1	64	36
0.50	0.95	225.6	−0.5	5.3	<0.1	70	30
0.70	0.60	226.3	−1.2	4.6	<0.1	68	32
0.80	0.36	225.9	−1.6	4.1	<0.1	72	28

significantly larger than the experimentally observed value of -1.7 cm^{-1} for the ^{57}Fe−^{54}Fe shift. The fact that Fe−L mode has an isotope shift pattern similar to that seen in the experiments strongly suggests that the force constants are in the range of 0.7−1.0 mdyn/Å for both Fe−L and Fe−P axial displacements. Moreover, the three-body analysis is consistent with the experimental observation that there is only one axial ligand mode in most spectra, and therefore, the predominantly Fe−P (doming) mode is presumably too low in frequency to be observed.[37,38]

Six-Body Model of the Iron−Ligand Out-of-Plane Mode. The linear three-body model does not include the bending force constants about the heme iron. These are included in a model of C_{4v} symmetry of the domed heme−iron complex in a six-body configuration, shown in Figure 1B. To be consistent with the three-body model, the masses are set to those of pyrrole groups ($m_1-m_4 = 122$ amu—i.e., the sum of masses m_1-m_4 gives 488 amu), iron groups ($m_5 = 56$), and imidazole groups ($m_6 = 68$) as before. In addition to stretching force constants of 1.68 mdyn/Å, a bending force constant of 0.25 mdyn $Å^{-1}$ rad^{-1} was also included. In particular, the value for the N_p−Fe−N_ϵ bend was set at 0.25 based on the N_p−Ni−N_p bend in NiOEP.[25,39,40] There are 12 normal modes in this system. They span $3A_1 + 2B_2 + 1B_2 + 3E$ irreducible representations in C_{4v}. According to the symmetry requirement of porphyrin, distortions along the z-axis can give rise to coupling between axial ligands and the π system of the porphyrin ring, and hence, Raman activity will be enhanced by a $\pi-\pi^*$ transition. In the D_{4h} symmetry of porphyrin, distortions along the z-axis are A_{2u} in symmetry, which transforms as A_1 in the C_{4v} point group. Hence, only the three A_1 modes can be Raman active by a mechanism that involves the overlap of the iron d_{z^2} orbitals with the a_{2u} orbital of the porphyrin. [1] In addition to in-phase and out-of-phase combinations of Fe−N_ϵ and Fe−N_p stretching and iron−porphyrin doming, there is a totally symmetric breathing mode.

A model that uses the force constants f(Fe−N_ϵ) = f(Fe−N_p) = 1.68 mdyn/Å produces a frequency of 341 cm^{-1} with a PED of 74% for the Fe−N_ϵ coordinate. As shown by the three-body model, the frequency is too high, and isotope shifts are incorrect for a model with an axial force constant larger than ~1 mdyn/Å. We consider decreasing the Fe−N_ϵ force constant while leaving the equatorial Fe−N_p force constants equal to f(Fe−N_p) = 1.68 mdyn/Å. The experimental frequency of ~225 cm^{-1} is only approached for an Fe−N_ϵ force constant of 0.4 mdyn/Å. This signifies an extremely weak bond, and the PED of the Fe−N_ϵ stretch falls to 18% for the 225 cm^{-1} mode, indicating that it is predominately a doming mode and not an axial ligand stretching mode. The consequence is that the isotope effects in the data are not reproduced for this set of force constants.

Much better agreement with the experiment is achieved if the axial and equatorial iron−ligand force constants are nearly equal [f(Fe−N_ϵ) ≈ f(Fe−N_p)]. The results of isotope effect calculations for these A_1 modes with force constants of 0.8 mdyn/Å (equatorial) and 0.6 mdyn/Å (axial) are shown in Table 5. Note that the pyrrole nitrogen $^{15}N_p$ isotope effect is again small for the axial-ligand out-of-plane modes; however, they do show up in the in-plane modes (not shown in the Table; see Supporting Information). The observed d_3-Im isotope shift is reproduced. However, as was found for the three-body model, the calculated ^{54}Fe isotope effect is substantially larger than that in the experiment.[2] We investigated the effect of including interaction force constant estimations based on the NiOEP force field.[25,42] Two normal modes that contain the Fe−Im stretch are found, and the trends observed are maintained as shown in Table 5.

Cβ-Subsituted 38-Body Porphyrin Model for Axially Ligated Heme. The experimental isotope shift of ^{54}Fe/^{57}Fe is not well reproduced by any of the above models. Although the C_{4v} six-body model does give insight into the type of normal modes that can be expected, it still does not include the effects of the low-frequency heme modes such as the doming of the porphyrin itself.[43,44] The six-body model does not allow for interactions between hindered ligands such as 2-methyl imidazole and the porphyrin.[45] Finally, this model does not include the internal coordinates of the axial ligand that may contribute to the axial normal mode.[3] A 38-body model that can be compared to the three-body and six-body models includes iron doming and off-axis tilting of the axial ligand. The point of this model is not to be inclusive of all effects, since the problem is underdetermined. Rather, the factors that agree with experimental data consistent with the simple three-body and six-body models will be emphasized.[46] The masses of the atoms are treated as pseudoatoms that include hydrogen masses, since high-frequency vibrational modes are not relevant to the problem at hand (Supporting Information). The magnitude of both out-of-plane $C_\alpha-N_p$−Fe and $C_{im}-N_\epsilon$−Fe bending coordinates was varied from 0.25 to 0.4 mdyn/Å/rad in model calculations.[25,39] In-plane bends of the porphyrin and imidazole ring are in the range of $0.8 \le \theta$(C−X−Y) ≤ 1.4 mdyn/$Å^{-1}$/$rad^{-1}$where X and Y can be any combination of C and N atoms. The parameters used for the bending and stretching coordinates of the imidazole were estimated on the basis of pyrrole values in the heme.[25] These are crude estimates, and no attempt has been made to model the high frequency modes correctly using this model. The model is intended to show trends in parameters that were used in the six-body model when ligand tilting and ring geometry are included.

Model calculations to extend the results from the three-body and six-body models were performed with a fixed NiOEP force field and variable stretching—f(Fe−N_ϵ) and f(Fe−N_p)—and bending—θ(N_p−Fe−N_ϵ)—force constants. The results of a FG matrix calculation performed using the program SVIB are shown in Table 6. On the basis of the PED of f(Fe−N_ϵ) there are more than three modes that have a significant iron−imidazole stretching character (see column 5 of Table 6). There are two symmetry classes of normal modes found to involve some amount of heme−ligand stretching. We call these A and B to represent their respective symmetries. The remaining modes (not shown in Table 6) are pure in-plane modes of the porphyrin ring or ligand bending modes (i.e., not pivoting on the iron but on the imidazole nitrogen N_ϵ). When the entire porphyrin ring is included, the character of the modes is slightly different than that of the six-body model. The mode with greatest contribution from iron−ligand stretching to the PED (50−70%) also has significant heme doming character (mode A in Table 6). The mode with next greatest iron−ligand stretching character (15−25% of the PED) also has significant ring-breathing character (mode A' in Table 6). This may represent involvement of the

TABLE 5: Force Constants, Frequencies, Isotope Shifts, and Potential Energy Distributions for the Six-Body Model[a]

force constants			isotopic wavenumber shifts (cm^{-1})				%PED		
f(Fe−L)	f(Fe−N_p)	f_θ	ν	d_3-Im	^{57}Fe−^{54}Fe	^{15}Np	Fe−L	Fe−Np	q
0.8	0.8	0.25	225.6	−1.6	4.0	−0.0	71	6	23
0.7	1.6	0.25	225.6	−1.4	4.0	−0.35	66	12	22
0.65	1.85	0.25	225.6	−0.8	3.9	−0.1	63	16	22
0.6	2.0	0.25	225.0	−0.6	3.7	−0.2	59	19	21
0.5	2.25	0.25	225.2	−0.3	3.2	−0.4	53	27	20
0.7	0.9	0.5	225.1	−1.2	4.4	0.0	68	6	26
0.6	1.65	0.5	225.4	−0.7	4.3	−0.1	62	13	25

[a] The wavenumber of the predominantly Fe−N_ϵ stretching vibrational mode is shown for various force constants. The calculation is derived from the A_1 matrix by the reduction of the six-body model using group theory.

TABLE 6: Frequencies and Isotope Shifts for a 38-Body Octa-substituted Porphyrin Including Only Stretching and Bending Force Constants[a]

Na	^{15}Np	^{54}Fe−^{57}Fe	d_3 Im	Na	
ν	$\Delta\nu$	$\Delta\nu$	$\Delta\nu$	% f(Fe−N_ϵ)	description
Parameters: f(Fe−N_ϵ) = 1.0, f(Fe−N_p) = 1.0, Bend = 0.25					
237.4	−0.2	3.8	−1.6	68	*A**
228.7	−0.1	1.7	−2.9	0	*B*
207.9	−0.4	0.1	−0.2	0	*A′*
103.9	−2.4	0.1	−0.6	11	*A″*
Parameters: f(Fe−N_ϵ) = 0.9, f(Fe−N_p) = 1.0, Bend = 0.25					
230.1	+0.7	2.5	−0.9	24	*B**
226.3	−0.1	2.8	−2.4	45	*A**
207.2	−0.5	0.2	−0.2	7	*A′*
103.3	−2.4	0.2	−0.6	12	*A″*
Parameters: f(Fe−N_ϵ) = 0.8, f(Fe−N_p) = 1.0, Bend = 0.25					
229.8	−0.2	1.8	−2.4	0	*B*
219.1	−0.3	3.0	−1.4	53	*A*
205.7	−0.3	0.7	−0.6	20	*A′*
102.4	−2.3	0.1	−0.6	14	*A″*
Parameters: f(Fe−N_ϵ) = 0.9, f(Fe−N_p) = 0.9, Bend = 0.25					
228.7	−0.2	3.4	−1.4	51	*A**
224.3	−0.2	2.2	−2.7	19	*B**
206.2	−0.4	0.2	−0.3	6	*A′*
103.1	−2.3	0.1	−0.6	12	*A″*
Parameters: f(Fe−N_ϵ) = 0.8, f(Fe−N_p) = 1.7, Bend = 0.25					
242.9				0	*B*
224.7	−0.4	3.9	−1.1	33	*A*/*A′* mixed
208.6	−0.3	2.3	−2.4	41	*A′*/*A* mixed
103.2	−2.6	0.0	−0.9	25	*A″*
Parameters: f(Fe−N_ϵ) = 0.8, f(Fe−N_p) = 0.9, Bend = 0.40					
228.7	−0.4	3.5	−1.1	44	*A**
225.1	−0.3	2.3	−1.4	14	*B**
205.9	−0.3	0.2	−0.1	0	*A′*
120.2	−2.5	0.0	−0.8	25	*A″*

[a] Mode description: *B*, ligand tilting (*B** includes iron−ligand stretching); *A*, iron−ligand stretching and heme−iron doming (*A**, includes ligand tilting); *A′*, iron−ligand stretching and ring breathing; *A″*, sombrero.

same internal coordinates observed in low-frequency totally symmetric modes such as ν_8 or ν_9 in the axial ligand stretch. Finally, there is a mode that includes iron−porphyrin axial out-of-phase motion (a sombrero mode) and some iron−ligand stretching (mode *A″* in Table 6). The sombrero mode at 110 cm^{-1} is consistent with the γ_8 mode found in earlier calculations of out-of-plane modes in NiOEP. [39] The *A* and *A′* modes have axial symmetry and can interact by Fermi resonance. The overtone of mode *A″* is in the 200−230 cm^{-1} region of the *A* and *A′* modes, and it can couple anharmonically with those modes.

There are also modes of *B*-type symmetry that include the C_{im}−N_ϵ−Fe bending coordinate. The most significant *B* modes in Table 6 have a contribution by Fe−N_ϵ stretching to the PED. The type-*B* modes in Table 6 that also show the greatest contribution of Fe−N_ϵ stretching to the PED. Modes of pure *B* symmetry are not Raman active except by vibronic coupling and will be considered in detail elsewhere.[52] There are three modes of *B* symmetry that are not included in Table 6. One of these is likely ν_{18} (a B_{1g} mode in the D_{4h} point group that is observed in NiOEP). There are also two low-frequency modes in 138−152 cm^{-1} range that involve the asymmetric out-of-plane motions of the pyrrole nitrogens and ligand tilting. These modes are mentioned because any detailed analysis of the nontotally symmetric modes in the low-frequency region must consider both in-plane and out-of-plane contributions. These issues are considered further in future studies of anharmonic coupling.[52]

Normal modes that involve both Fe−N_ϵ stretching and θ-(C_{im}−N_ϵ−Fe) bending show a ^{54}Fe−^{57}Fe isotope effect that agrees best with experiment. In the model calculation with f(Fe−N_ϵ) ≈ 0.8 mdyn/Å and f(Fe−N_p) ≈ 1.0 mdyn/Å, the isotope shifts for ^{54}Fe and d_3-Im, and the $^{15}N_p$ shift are in the correct range for the highest-frequency mode 230 cm^{-1} (mode *A**). A mode with larger bending character (also labeled type *B** in Table 6) is found to be only 5 cm^{-1} lower in energy. Both *A** and *B** modes are marked with asterisks to indicate that these modes contain both ligand stretching and tilting internal coordinates. The extent of this mixing does depend on the parameters as shown by comparing the calculation with f(Fe−N_ϵ) ≈ 0.9 mdyn/Å and f(Fe−N_p) ≈ 1.0 mdyn/Å, where no mixing of bending and stretching occurs. Raman activity can be introduced by changes in electron density in the d_{z^2} orbital by axial ligand stretching, but ligand bending may also affect the overlap of d_{z^2} with orbitals of the protoporphyrin IX ring, and thus, both modes may be simultaneously Raman active.[41] The present study indicates that the bending internal coordinates of the imidazole does not contribute strongly to the PED of the axial-ligand out-of-plane mode.[3] The analysis suggests that a mode involving heme doming and iron−ligand stretching accounts for the isotope data in H93G(Im) and H93G(Pyr) and is consistent with the data obtained in isotopically labeled sperm whale myoglobin.

The fact that two or more modes are in the same frequency range raises the possibility that the Fe−His mode is a composite of more than one vibrational mode in the energy range from 210 to 230 cm^{-1}. Line shape analysis suggests that there is more than one Raman active band in the spectral region of the out-of-plane vibration.[47] The present calculation suggests that multiple Raman active modes can be isoenergetic but have different stretching and bending character. These considerations are of interest for the H93G(2-Me Im) and H93G(N-Me Im) adducts where anharmonic coupling involving normal modes of the appropriate symmetry may be important.[52]

Anharmonicity of the Iron−Ligand Out-of-Plane Mode. The differences in the isotope effects of H93G(N-Me Im), H93G(2-Me Im), and H93G(Im) cannot be accounted for by a

normal mode calculation. The isotope effect of either dideuteration or ^{15}N substitution of N-Me Im in H93G(d_2-N-Me Im) or H93G(1,3-di-^{15}N N-Me Im), respectively, would be expected to be small on the basis of the above considerations for the imidazole isotopomers in H93G(Im). The X-ray crystal structure data and NMR data on the metaquo and metcyano forms, respectively, show that N-Me Im and Im have nearly identical orientations in the proximal ligand pocket.[49] The difference in their pK_a values, 7.33 and 6.65, respectively (see Table 1), is small. However, in H93G(N-Me Im), the N-Me Im cannot form a hydrogen bond to serine 92, as observed in H93G(Im) and H93G(4-Me Im).[49]

The isotope effect in H93G(N-Me Im) is attributable to Fermi resonance. The splitting of the vibrational mode frequency into two frequencies (one higher and one lower) can occur if an overtone or combination of low-frequency modes has the same energy and symmetry as that of the iron−axial-ligand mode. The fact that two independent isotope measurements result in the collapse of these two frequencies into one which is very nearly the average of the two suggests that a Fermi resonance effect involving a significant coupling of $\sim$7 cm^{-1} is responsible.[50] The other conceivable explanation that there are two or more conformations has been proposed for wild-type myoglobin.[47] However the existence of more than one conformation of the N-Me Im ligand in the proximal cavity of H93G is not consistent with the X-ray crystal structure,[49] the NMR data, or the isotope effects presented here.

Although we have no structural data for H93G(2-Me Im), this adduct is likely to have significant steric interactions with the porphyrin ring of the heme. With the harmonic approximation, no amount of strain appears to account for the large observed isotope effect,[51] and therefore, we suggest that the isotope shift of 2-Me Im in Figure 4 is most likely explained by its large anharmonicity. Measurements of the temperature dependence of the frequency of the axial-ligand vibrational modes for a number of different ligands presented elsewhere[52] show differing anharmonicity for different ligands. The ligand with the largest anharmonic coupling is H93G(2-Me Im).[53]

For anharmonic coupling to exist, there must be low-frequency modes that can couple to the iron−ligand mode.[54] One obvious candidate is the sombrero mode (mode *A″* in Table 6). For example, the overtone of mode that has doming character is in the correct range to couple by Fermi resonance. Additionally, bending modes may be important particularly if the observed normal mode has bending character (e.g., mode *B* in Table 6). In hindered ligands, bending interactions are likely to be larger, and this may explain the observed isotope effects. In summary, we find that the inclusion of a bending internal coordinate within the harmonic approximation does not account for the observed isotope effects.[51] By contrast, the ansatz proposed here is that anharmonic coupling of low-frequency normal modes with strong bending character is likely to be important for strained iron−ligand conformations.

Comparison of Axial Ligands. The data presented in Figure 2 and Table 1 show a range of frequencies for different ligands. To properly compare the observed frequencies and pK_a's of different ligands, we used the three-body model in eq 1 to obtain the correlation shown in Figure 6. To obtain the appropriate Fe−L force constant, we held the Fe−N_p force constant constant at a value of 0.78 mdyn/Å, consistent with the calculation for the Im ligand given in row 2 of Table 4. The force constant for the Fe−L coordinate was obtained for the various molecular masses (m_1, shown in column 4 of Table 1) by fitting the f_{12} [f(Fe−L)] force constant to the observed resonance Raman frequency using eq 1. Figure 6 shows that for ligands with pK_a > 5, the frequency of the mode is roughly proportional to pK_a. In fact, for the ligands shown, there is a good linear correlation for all the alkyl-substituted imidazoles and pyridine (fit not shown). However, the 3-bromo- and 3-fluoropyridine frequencies do not lie on the line, and the data are shown fit to a quadratic function (f(Fe−L) = 0.47−0.036pK_a + 0.007pK_a2).[55] It is possible that the decrease in ligand basicity results in a cis effect that strengthens the Fe−N_p bond, thus changing the contribution of the iron−ligand stretch in the normal mode.

An alternative explanation is that the effective pK_a of the ligand in the proximal pocket is significantly modified compared to the value in solution. Such effects are well-known for amino acids where large pK_a shifts are common in the interior of proteins. The effect may also be related to the effect of redox stabilization observed in the H93G protein. Redox stabilization is based on the observed lack of a large shift in redox potential for a series of ligands whose solution redox potentials show shifts of several hundred millivolts.[56] Redox stabilization may also be the effect that stabilizes thiolate ligation in cytochrome P450[57] and imidazolate ligation in cytochrome *c* peroxidase.[58] The same environmental effect in the protein that leads to a stabilization of the redox potential may lead to a stabilization of the ligation of iron in the ferrous form, and this electrostatic environmental effect could affect the resonance Raman frequency.[59]

Conclusion

There is increasing evidence that the frequency of the axial-ligand out-of-plane mode is modulated by factors other than the strength of the iron−ligand bond. The normal-mode analysis indicates that the motion of the iron with respect to the porphyrin and bending of the axial ligand are nearly as important as the iron−ligand stretch. Anharmonic coupling of the 200−245 cm^{-1} Raman active mode to low-frequency modes is quite possible, given the existence of low-frequency doming modes.[44] These results have implications for the observed correlation of the mode frequency with oxygen binding affinity and oxygen bond cleavage reactivity. The observed frequency reduction of the Fe−His mode in T-state hemoglobin may result from anharmonic coupling to low-frequency bending modes. This proposal differs subtly from the proposals concerning the origin of the frequency lowering of the Fe−His in T-state compared to R-state hemoglobin.[6] It suggests that strain may not be exclusively due to a protein pulling on the axial ligand but can also occur through controlling the heme structure and flexibility. The comparison of a number of ligands to heme iron in the proximal cavity mutant also supports the correlation of reactivity with ligand basicity. This correlation is important for explaining the frequency range of the iron−histidine out-of-plane mode in native heme proteins: oxidases (200−215 cm^{-1}), globins (215−225 cm^{-1}), and peroxidases (240−245 cm^{-1}).[8] The three-body model used to obtain corrections for the mass of different ligands appears to have validity for the substituted imidazole and pyridine ligands studied here. The three-body model is analytic (eq 1) and can be used instead of the two-body harmonic oscillator model for the iron−histidine mode to account for the effects of ligand basicity or strain. The 6- and 38-body models show that ligand bending may also play an important role; however, the number of degrees of freedom is large, leading to a variety of possible interpretations of the data. These models are consistent in their indication of a role for the off-axis bending and coupling of totally symmetric in-plane modes. All of the model calculations indicate that the motion of the iron relative

to the porphyrin contributes significantly to the potential energy distribution in the observed axial-ligand out-of-plane vibration.

Acknowledgment. S.F. was supported by a Los Alamos Director's Fellowship that made this work possible. The authors thank Dr. J. Shelnutt for stimulating conversations. The authors thank Dr. S. Decatur for preparation of H93G myoglobin.

Supporting Information Available: Normal coordinate analysis for 3-body, 6-body, and 38-body porphyrin models, sample input file for the SVIB program relevant to the data presented, and sample fits and tables of fitted functions used. This material is available free of charge via the Internet at http://pubs.acs.org.

References and Notes

(1) Kitagawa, T.; Nagai, K.; Tsubaki, M. *FEBS Lett.* **1979**, *104*, 376−378.

(2) Argade, P. V.; Sassaroli, M.; Rousseau, D. L.; Inubushi, T.; Ikeda-Saito, M.; Lapidot, A. *J. Am. Chem. Soc.* **1984**, *106*, 6593−6596.

(3) Wells, A. V.; Sage, T. J.; Morikis, D.; Champion, P. M.; Chiu, M. L.; Sligar, S. G. *J. Am. Chem. Soc.* **1991**, *113*, 9655−9660.

(4) Barrick, D. *Biochemistry* **1994**, *33*, 6546−6554.

(5) DePillis, G.; Decatur, S. M.; Barrick, D.; Boxer, S. G. *J. Am. Chem. Soc.* **1994**, *116*, 6981−6982.

(6) Friedman, J. M.; Scott, T. W.; Stepnowski, R. A.; Ikeda-Saito, M.; Yonetani, T. *J. Biol. Chem.* **1983**, *258*, 10564−10572.

(7) Shelnutt, J. A.; Alden, R. G.; Ondrias, M. R. *J. Biol. Chem.* **1986**, *261*, 1720−1733.

(8) Spiro, T. G.; Smulevich, G.; Su, C. *Biochemistry* **1990**, *29*, 4497−4508.

(9) Woodruff, W. H.; Einarsdottir, O.; Dyer, R. B.; Bagley, K. A.; Palmer, G.; Atherton, S. J.; Goldbeck, R. A.; Dawes, T. D.; Kliger, D. S. *Proc. Natl. Acad. Sci. U.S.A.* **1991**, *88*, 2588−2592.

(10) Ondrias, M. R.; Friedman, J. M.; Rousseau, D. L. *Science* **1983**, *220*, 615−617.

(11) Matsukawa, S.; Mawatari, K.; Yoneyama, Y.; Kitagawa, T. *J. Am. Chem. Soc.* **1985**, *107*, 1108−1113.

(12) Teraoka, J.; Kitagawa, T. *J. Biol. Chem.* **1981**, *256*, 3969−3972.

(13) Yamaguchi, K.; Watanabe, Y.; Morishima, I. *Inorg. Chem.* **1992**, *31*, 156−157.

(14) Zhao, Y.; Schelvis, J. P. M.; Babcock, G. T.; et al. *Biochemistry* **1998**, *37*, 4502−4509.

(15) Oertling, W. A.; Surerus, K. K.; Einarsdottir, O.; Fee, J. A.; Dyer, R. B.; Woodruff, W. H. *Biochemistry* **1994**, *33*, 3128−3141.

(16) Ogura, T.; Hon-nami, K.; Oshima, T.; Yoshikawa, S.; Kitagawa, T. *J. Am. Chem. Soc.* **1983**, *105*, 7781−7783.

(17) Tsukihara, T.; Aoyama, H.; Yamashita, E.; Tomizaki, T.; Yamaguchi, H.; Shinzawa-Itoh, K.; Nakashima, R.; Yaono, R.; Yoshikawa, S. *Science* **1995**, *269*, 1069−1074.

(18) Iwata, S.; Ostermeier, C.; Ludwig, B.; Michel, H. *Nature* **1995**, *376*, 660−669.

(19) Sun, J.; Fitzgerald, M. M.; Goodin, D. B.; Loehr, T. M. *J. Am. Chem. Soc.* **1997**, *119*, 2064−2065.

(20) Newmeyer, S. L.; Sun, J.; Loehr, T. M.; Ortiz de Montellano, P. R. *Biochemistry* **1996**, *35*, 12788−12795.

(21) Sun, J.; Loehr, T. M.; Wilks, A.; Ortiz de Monellano, P. R. *Biochemistry* **1994**, *33*, 13734−13740.

(22) Hu, S.; Smith, K. M.; Spiro, T. G. *J. Am. Chem. Soc.* **1996**, *118*, 12638.

(23) Christian, J. F.; Unno, M.; Sage, J. T.; Champion, P. M.; Chien, E.; Sligar, S. G. *Biochemistry*, submitted for publication.

(24) Wilson, E. B.; Decius, J. C.; Cross, P. C. *Molecular Vibrations*; Dover Publications Inc.: New York, 1955.

(25) Li, X. Y.; Czernuszewicz, R. S.; Kincaid, J. R.; Stein, P.; Spiro, T. G. *J. Phys. Chem.* **1990**, *94*, 47−61.

(26) Desbois, A.; Lutz, M. *Biochim. Biophys. Acta* **1981**, *671*, 168−176.

(27) Bangcharoenpaurpong, O.; Schomaker, K. T.; Champion, P. M. *J. Am. Chem. Soc.* **1984**, *106*, 5688−5698.

(28) Kitagawa, T. In *Biological Applications of Raman Spectroscopy*; Kitagawa, T., Ed.; 1988; Vol. III.

(29) Champion, P. M.; Stallard, B. R.; Wagner, G. C.; Gunsalus, I. C. *J. Am. Chem. Soc.* **1982**, *104*, 5469−5472.

(30) Shelnutt, J. A.; Alston, K.; Ho, J.-Y.; Yu, N.-T.; Yamamoto, T.; Rifkind, J. M. *Biochemistry* **1986**, *25*, 620−627.

(31) We have used the empirical relation $k = -\log((d - 1.55\ \text{Å})/0.899)/0.162$ to calculate the force constant k as a function of internuclear distance d.

(32) Hoard, J. L.; Scheidt, W. R. *Proc. Natl. Acad. Sci. U.S.A.* **1973**, 3919−3922.

(33) Fermi, G. *J. Mol. Biol.* **1975**, *82*, 371−391.

(34) Takano, T. *J. Mol. Biol.* **1977**, *110*, 569−584.

(35) Chance, M. R.; Miller, L. M.; Fischetti, R. F.; Scheuring, E.; Huang, W. X.; Sclavi, B.; Hai, Y.; Sullivan, M. *Biochemistry* **1996**, *35*, 9014−9023.

(36) Mitchell, M.; Li, X. Y.; Kincaid, J. R.; Spiro, T. G. *J. Phys. Chem.* **1987**, *91*, 4690−4696.

(37) Zhu, L.; Li, P.; Huang, M.; Sage, J. T.; Champion, P. M. *Phys. Rev. Lett.* **1994**, *72*, 301−304.

(38) Li, X.-Y.; Zgierski, M. Z. *Chem. Phys. Lett.* **1992**, *188*, 16−20.

(39) Li, X. Y.; Czernuszewicz, R. S.; Kincaid, J. R.; Spiro, T. G. *J. Am. Chem. Soc.* **1989**, *111*, 7012−7023.

(40) As noted in ref 25, the Np−Fe−Np bend and the Np(4)−Fe wag have the same internal coordinates. We use the bend definition here.

(41) Stavrov, S. S. *Biophys. J.* **1993**, *65*, 1942−1950.

(42) Piffat, C.; Melamed, D.; Spiro, T. G. *J. Phys. Chem.* **1993**, *97*, 7441−7450.

(43) Jentzen, W.; Song, X.-Z.; Shelnutt, J. A. *J. Phys. Chem. B* **1997**, *101*, 1684−1699.

(44) The sombrero mode in Table 6 is not the lowest-frequency doming mode possible. The calculation did not include heme torsional coordinates that would give rise to the low-frequency out-of-plane modes of the macrocycle itself. The present model is consistent with anharmonic coupling involving still lower-frequency modes. This issue was not examined for lack of experimental data to support detailed modeling.

(45) Schweitzer-Stenner, R.; Dreybrodt, W. *J. Raman Spectrosc.* **1992**, *23*, 539−550.

(46) The complexity of the 38-body model may seem unwarranted at first, given that there are 46 stretching force constants, 79 bending force constants, and a large number of torsional and wagging force constants that could be included. However, in the model calculation, the in-plane force constants are fixed, and all torsions, wags, and interaction force constants are ignored. The stretching and bending force constants for the imidazole ring in this calculation have been based on estimates from the pyrrole ring force constants for the in-plane force field (see Supporting Information). The goal of the calculations is to consider the essential degrees of freedom that contribute to an axial out-of-plane mode.

(47) Gilch, H.; Schweitzer-Stenner, R.; Dreybrodt, W. *Biophys. J.* **1993**, *65*, 1470−1485.

(48) Ahmed, A. M.; Campbell, B. F.; Caruso, D.; Chance, M. R.; Chavez, M. D.; Courtney, S. H.; Friedman, J. M.; Iben, I. E. T.; Ondrias, M. R.; Yang, M. *Chem. Phys.* **1991**, *158*, 329−351.

(49) Barrick, D.; Dahlquist, F. W. *Proteins: Struct., Funct., Genet.* **2000**, *39*, 278−290.

(50) Fermi, E. *Z. Phys.* **1931**, *71*, 250−259.

(51) We have investigated three-body models that include ligand bending within a harmonic approximation. Ligand bending is also included in the six-body and 38-body models. The result of these investigations is that there is no range of bending force constants that can explain the anomalous isotope effects in Figures 4 and 5 with a harmonic approximation.

(52) Franzen, S.; Fritsch, K.; Dyer, R. B.; Boxer, S. G.; Frauenfelder, H. Manuscript in preparation.

(53) The fact that axial ligand strain can result in significant frequency lowering due to anharmonic coupling is demonstrated also by a comparison of the frequency of 4-methyl imidazole in both H93G and the double mutant S92T/H93G (data not shown). There is clearly less volume in the proximal cavity of the S92T/H93G double mutant because of the methyl group of threonine. The presence of this methyl group has no apparent affect on the frequency of S92T/H93G(Im) or S92T/H93G(N-Me Im) but lowers the frequency of S92T/H93G(4-Me Im) by 10 cm^{-1} with respect to that of H93G(4-Me Im) (data not shown).

(54) Rosenfeld, Y. B.; Stavrov, S. S. *Chem. Phys. Lett.* **1994**, *229*, 457−464.

(55) Resonant Raman data for the H93G(4-Me Pyr) and S92T/H93G-(4-Me Im) adducts have not been included on the plot. In both of these cases, the ligands bind very weakly but not due to their low pK_a. In the case of the H93G(4-Me Pyr), adduct preparation requires reconstitution of H93G with heme since the ligand cannot be introduced by dialysis. We did not succeed in forming the 2-methyl- or 2-fluoropyridine adducts even with this procedure, suggesting that binding is very weak to deoxyferrous heme iron. It appears that in these cases steric hindrance results in a lowering of the frequency of the Raman mode. This has been suspected to be the origin of the lower frequency of 2-methyl imidazole adducts of iron porphyrins.

(56) Pang, P.; Boxer, S. G. Manuscript in preparation.

(57) Poulos, T. L.; Raag, R. *FASEB J.* **1992**, *6*, 674−679.

(58) Goodin, D. B.; McRee, D. E. *Biochemistry* **1993**, *32*, 3313−3324.

(59) Kushkuley, B.; Stavrov, S. S. *Biophys. J.* **1997**, *72*, 899−912.